

Magnetar Engines in Fast Blue Optical Transients and Their Connections with SLSNe, SNe Ic-BL, and IGRBs

JIAN-FENG LIU,^{1,2} JIN-PING ZHU^{ID},³ LIANG-DUAN LIU^{ID},^{1,2} YUN-WEI YU^{ID},^{1,2} AND BING ZHANG^{ID},^{4,5}

¹*Institute of Astrophysics, Central China Normal University, Wuhan 430079, China; yuyw@ccnu.edu.cn, liuld@ccnu.edu.cn*

²*Key Laboratory of Quark and Lepton Physics (Central China Normal University), Ministry of Education, Wuhan 430079, China*

³*Department of Astronomy, School of Physics, Peking University, Beijing 100871, China*

⁴*Nevada Center for Astrophysics, University of Nevada, Las Vegas, NV 89154, USA*

⁵*Department of Physics and Astronomy, University of Nevada, Las Vegas, NV 89154, USA*

ABSTRACT

We fit the multi-band lightcurves of 40 fast blue optical transients (FBOTs) with the magnetar engine model. The mass of the FBOT ejecta, the initial spin period and polar magnetic field of the FBOT magnetars are respectively constrained to $M_{\text{ej}} = 0.11^{+0.22}_{-0.09} M_{\odot}$, $P_1 = 9.1^{+9.3}_{-4.4}$ ms, and $B_p = 11^{+18}_{-7} \times 10^{14}$ G. The wide distribution of the value of B_p spreads the parameter ranges of the magnetars from superluminous supernovae (SLSNe) to broad-line Type Ic supernovae (SNe Ic-BL; some are observed to be associated with long-duration gamma-ray bursts), which are also suggested to be driven by magnetars. Combining FBOTs with the other transients, we find a strong universal anti-correlation as $P_1 \propto M_{\text{ej}}^{-0.41}$, indicating them could share a common origin. To be specific, it is suspected that all of these transients originate from collapse of extreme-stripped stars in close binary systems, but with different progenitor masses. As a result, FBOTs distinct themselves by their small ejecta masses with an upper limit of $\sim 1 M_{\odot}$, which leads to an observational separation in the rise time of the lightcurves ~ 10 d. In addition, the FBOTs together with SLSNe can be separated from SNe Ic-BL by an empirical line in the $M_{\text{peak}} - t_{\text{rise}}$ plane corresponding to an energy requirement of a mass of ^{56}Ni of $\sim 0.3 M_{\text{ej}}$, where M_{peak} is the peak absolute magnitude of the transients and t_{rise} is the rise time.

Keywords: Light curves (918); Magnetars (992); Supernovae (1668)

1. INTRODUCTION

In the past decade, several unique, fast-evolving and luminous transients have been discovered, thanks to the improved cadence and technology of wide-field surveys. These transients are usually quite blue ($g - r \lesssim -0.2$) and luminous (an absolute magnitude of $-16 \lesssim M_{\text{peak}} \lesssim -23$) at peak and their lightcurves show fast rise and decline with a duration shorter than about ten days. They are, hence, named as fast blue optical transients (FBOTs; e.g., Drout et al. 2014; Inserra 2019). Since Drout et al. (2014) reported a sample of FBOTs identified from a search within the Pan-STARRS1 Medium Deep Survey (PS1-MDS) data, the observations of ~ 100 FBOT candidates have been presented (e.g., Arcavi et al. 2016; Whitesides et al. 2017; Pursiainen et al. 2018; Tampo et al. 2020; Ho et al. 2019, 2020, 2021). The event rate density of FBOTs is $\sim 1 - 10\%$ of that of local core-collapse supernovae (SNe; Drout et al. 2014; Pursiainen et al. 2018; Ho et al. 2021).

The progenitor and energy source of FBOTs are still very unclear. Two different classes of models have been

proposed in literature to explain the observational properties of FBOTs. The first class broadly contains binary neutron star (BNS), binary white dwarf (BWD) or NS-WD mergers (e.g., Yu et al. 2013, 2015, 2019b; Zenati et al. 2019); accretion-induced collapse (AIC) of a WD (e.g., Kasliwal et al. 2010; Brooks et al. 2017; Yu et al. 2015, 2019a); SN explosions of ultra-stripped progenitor stars (e.g., Tauris et al. 2013, 2015, 2017; Suwa et al. 2015; Hotokezaka et al. 2017; De et al. 2018; Sawada et al. 2022) including electron capture SNe (e.g., Moriya & Eldridge 2016; Mor et al. 2022); common envelope jets SNe (Soker et al. 2019; Soker 2022); and tidal disruption of a star by a NS or a black hole (e.g., Liu et al. 2018; Perley et al. 2019; Kremer et al. 2021; Metzger 2022). The common feature of this class of models is that the fast evolution of FBOTs is attributed to a small ejecta mass, and the luminous brightness of FBOTs is attributed to additional energy injection from a central engine sources besides the radioactive decay power by ^{56}Ni (e.g., Drout et al. 2014; Pursiainen et al. 2018). The extra energy source could be a spinning-down NS

or an accreting black hole (i.e., in the tidal disruption models). The second class of models invoke shock breakouts from a dense stellar wind (e.g., [Chevalier & Irwin 2011](#); [Ginzburg & Balberg 2012](#); [Drout et al. 2014](#)); interaction between the ejecta from a massive star and a dense circumstellar material (CSM; e.g., [Rest et al. 2018](#); [Fox & Smith 2019](#); [Leung et al. 2020](#); [Xiang et al. 2021](#); [Pellegrino et al. 2022](#)); and jet-cocoon interaction and emission ([Gottlieb et al. 2022](#)). FBOTs in this class of models are attributed to the breakout of the accumulated energy in the shock. By fitting the bolometric light curves of FBOTs with the CSM interaction plus ^{56}Ni decay model, [Xiang et al. \(2021\)](#) and [Pellegrino et al. \(2022\)](#) found that, in order to account for the rapid and luminous light curves, the mass loss rates of the progenitor should be up to $\sim 1M_{\odot} \text{ yr}^{-1}$, which is however inconsistent with the limits obtained from the radio observations of FBOTs.

Recent studies revealed that the hosts of FBOTs are exclusively star-forming galaxies ([Drout et al. 2014](#); [Pursiainen et al. 2018](#); [Pellegrino et al. 2022](#)), whose star-formation rates and metallicities are consistent with those of extreme stripped-envelope explosions ([Wiseman et al. 2020](#)) including hydrogen-poor Type Ic superluminous SNe (SLSNe; e.g., [Lunnan et al. 2014](#); [Chen et al. 2017](#)), broad-lined Type Ic SNe (SNe Ic-BL; e.g., [Arcavi et al. 2010](#)), and long-duration gamma-ray bursts (LGRBs; e.g., [Krühler et al. 2015](#); [Perley et al. 2016](#)). Furthermore, it is worth noticing that these extreme stripped-envelope explosions are widely believed to harbor a long-lived millisecond magnetar ([Dai & Lu 1998](#); [Wheeler et al. 2000](#); [Zhang & Mészáros 2001](#); [Yu et al. 2010](#); [Kasen & Bildsten 2010](#); [Woosley 2010](#); [Piro & Ott 2011](#); [Inserra et al. 2013](#); [Zhang 2018](#)), which can lose its rotational energy via spin-down processes to provide an additional energy injection for the explosion. Therefore, in view of the similarity between the host galaxies of FBOTs and those of SLSNe, SNe Ic-BL, and LGRBs, it would be reasonable to suspect that the FBOTs are also powered by a magnetar engine. Indeed, the existence of such an engine can provide a good explanation to the lightcurves of some FBOTs ([Yu et al. 2015](#); [Hotokezaka et al. 2017](#); [Rest et al. 2018](#); [Margutti et al. 2019](#); [Wang et al. 2019](#); [Sawada et al. 2022](#)).

In addition, the benchmark FBOT event, AT2018cow, from a nearby luminosity distance $\approx 60 \text{ Mpc}$ ([Prentice et al. 2018](#); [Perley et al. 2019](#)) provided an opportunity for the broad-band observations from radio to γ -rays ([Rivera Sandoval et al. 2018](#); [Ho et al. 2019](#); [Margutti et al. 2019](#); [Huang et al. 2019](#)). In particular, the radio observation revealed a dense magnetized environment of AT2018cow, which plausi-

bly supports the existence of a newly formed magnetar ([Mohan et al. 2020](#)).

Based on the above considerations, in this paper, we collect a large number of FBOTs from the literature and fit their light curves within the framework of the magnetar engine model. The obtained parameters are further compared with those of SLSNe and SNe Ic-BL associated/unassociated with LGRBs. Previously, [Yu et al. \(2017\)](#) had suggested a united scenario to connect SLSNe and SNe Ic-BL. Therefore, in this paper, we will investigate whether such a united understanding can be extended to the FBOT phenomena, which could provide a key rule to the physical origin of the FBOTs.

2. LIGHTCURVE MODELING

2.1. Sample Selection

The criteria for our sample selections are as follows: (1) reported rise time above half-maximum $t_{\text{rise}} \lesssim 10 \text{ d}$, (2) spectroscopic redshift measurement from its host galaxy spectral features; (3) published lightcurves observed in at least two filters; (4) at least some data are available close to the peak.

Following the above criteria, we collect 40 FBOTs from the literature: 7 events from the PS1-MDS ([Drout et al. 2014](#); [Inserra 2019](#)); 25 events reported in the Dark Energy Survey Supernova Program (DES-SN; [Pursiainen et al. 2018](#)); 3 events collected from the Supernova Legacy Survey (SNLS; [Arcavi et al. 2016](#)); 2 events discovered by the Hyper Suprime-Cam SSP (HSC-SSP) Transient Survey ([Tampo et al. 2020](#)); and 3 well studied samples, i.e., PTF10iam, AT2018cow, and Koala, discovered by the Palomar Transient Factory (PTF; [Arcavi et al. 2016](#)), the Asteroid Terrestrial-impact Last Alert System (ATLAS) Survey ([Prentice et al. 2018](#); [Perley et al. 2019](#)), and the Zwicky Transient Facility One-d Cadence (ZTF-1DC) Survey ([Ho et al. 2020](#)), respectively.

Our FBOT sample contains 22 robust cases whose rises were recorded in survey projects. For these events, sufficient data on the rise and decline phases of the lightcurve pose a strict constraint on the model parameters, especially for the ejecta mass. The sample also includes 18 events without any detection during the rise phase of the lightcurve. Due to the lack of observational epoch before the peak, the model parameters are related to the rise time we set.

2.2. Magnetar Engine Model

As usual, the spin-down luminosity of a magnetar can be generally expressed according to the luminosity of magnetic dipole radiation as

$$L_{\text{sd}}(t) = L_{\text{sd},i} \left(1 + \frac{t}{t_{\text{sd}}}\right)^{-2}, \quad (1)$$

where $L_{\text{sd},i} = 10^{47} \text{ erg s}^{-1} P_{i,-3}^{-4} B_{p,14}^2$ is the initial value of the luminosity, $t_{\text{sd}} \simeq 2 \times 10^5 \text{ s } P_{i,-3}^2 B_{p,14}^{-2}$ is the spin-down timescale, and P_i and B_p are the initial spin period and polar magnetic strength of the magnetar, respectively. The total rotational energy of the magnetar can be written as $E_{\text{rot}} = L_{\text{sd},i} t_{\text{sd}} = 2 \times 10^{52} \text{ erg } P_{i,-3}^{-2}$. Here the conventional notation $Q_x = Q/10^x$ is adopted in cgs units.

We adopt the common analytic solution derived by [Arnett \(1982\)](#) to calculate the bolometric luminosity of an FBOT powered by a magnetar as:

$$L_{\text{rad}}(t) = e^{-(t/t_{\text{diff}})^2} (1 - e^{-At^{-2}}) \times \int_0^t 2L_{\text{sd}}(t') \frac{t'}{t_{\text{diff}}} e^{(t'/t_{\text{diff}})^2} \frac{dt'}{t_{\text{diff}}}, \quad (2)$$

where t_{diff} is the photon diffusion timescale of the FBOT ejecta and A is the leakage parameter. For an ejecta of a mass M_{ej} and velocity v_{ej} , the diffusion timescale is given by $t_{\text{diff}} = (3\kappa M_{\text{ej}}/4\pi v_{\text{ej}} c)^{1/2}$, where κ is the optical opacity. Here the dynamical evolution of the ejecta is ignored. The kinetic energy of the ejecta is assumed to be directly determined by the rotational energy of the magnetar so that the ejecta velocity can be estimated as $v_{\text{ej}} \simeq \sqrt{2E_{\text{rot}}/M_{\text{ej}}}$. This assumption is viable as long as $t_{\text{sd}} \lesssim t_{\text{diff}}$ and the initial value of the kinetic energy is not much higher than 10^{50} erg ¹. By considering that the energy injected into the ejecta could be in the form of high-energy photons, we write the leakage parameter of the ejecta as $A = 3\kappa_{\gamma} M_{\text{ej}}/4\pi v_{\text{ej}}^2$, where κ_{γ} is the opacity for gamma-rays. The frequency-dependence of κ_{γ} is ignored for simplicity.

Finally, in order to calculate the monochromatic luminosity of the FBOT emission, we define an photosphere temperature as

$$T_{\text{ph}}(t) = \max \left[\left(\frac{L_{\text{rad}}}{4\pi\sigma_{\text{SB}} v_{\text{ph}}^2 t^2} \right)^{1/4}, T_{\text{floor}} \right] \quad (3)$$

¹ The explosion energy of a typical SNe Ib/c is around 10^{51} erg ([Ugliano et al. 2012](#); [Ertl et al. 2016](#)). However, for FBOTs, if they mostly originate from ultra-stripped SNe as suggested below, then it could be natural to expect a relatively weak explosion. In this case, it would be simple and reasonable to assume that the final kinetic energy of the FBOT ejecta is determined by the injected energy (i.e., the rotational energy of the magnetar).

Table 1. Fitting Parameters and Priors

Parameter	Min	Max	Prior
M_{ej}/M_{\odot}	0.001	20	Log-flat
P_i/ms	0.5	50	Log-flat
B_p/G	10^{13}	10^{17}	Log-flat
$\kappa/\text{cm}^2 \text{ g}^{-1}$	0.01	0.2	Flat
$\kappa_{\gamma}/\text{cm}^2 \text{ g}^{-1}$	10^{-2}	10^2	Log-flat
$T_{\text{floor}}/10^3 \text{ K}$	3	25	Flat
$t_{\text{shift}}/\text{d}$	0	20	Flat
A_V/mag	0	0.5	Flat

with the Stefan-Boltzmann constant σ_{SB} , floor temperature T_{floor} , and photospheric velocity $v_{\text{ph}} \simeq v_{\text{ej}}$ (which is a standard approximation in the literature).

2.3. Lightcurve Fitting

By adopting a Markov Chain Monte Carlo method, we use the magnetar engine model described in Section 2.2 with the `emcee` package ([Foreman-Mackey et al. 2013](#)) to fit the multi-band lightcurves of the collected FBOTs. For the Milky Way extinction, we take values from the dust maps of ([Schlafly & Finkbeiner 2011](#)) and fix $R_V = 3.1$. Because the extinction of the host galaxy is unknown, we set A_V as a free parameter, with a uniform distribution prior between 0 and 0.5 magnitudes. There are 8 free parameters: ejecta mass M_{ej} , initial spin period P_i , magnetic field strength B_p , opacity κ , opacity to high-energy photons κ_{γ} , floor temperature T_{floor} , host extinction A_V , and the time of explosion relative to the first observed data point t_{shift} . [Ho et al. \(2021\)](#) recently reported 22 FBOTs with spectroscopic observations, most of which were classified as Type Ib/Ibn/IIf SNe or hybrid IIn/Ibn SNe. Furthermore, a fraction of FBOTs were found to be Type Ic SNe (e.g., [Drout et al. 2013](#); [De et al. 2018](#)). Although a major fraction of FBOTs lack spectroscopic classifications, we assume that these collected FBOTs could plausibly contain a large amount of helium, carbon or oxygen. Thus, the prior of κ for FBOTs is preferably set in a range of $0.05 - 0.2 \text{ cm}^2 \text{ g}^{-1}$, which is suitable for scattering in ionized helium, carbon or oxygen. For those events without any detection before the peak, we note that the upper limit of the prior for t_{shift} is defined as the time between the pre-explosion non-detection and the first detection. The priors of these fitting parameters are listed in Table 1.

For each lightcurve fitting, we run the code in parallel using 12 nodes with at least 10,000 iterations where the

first 100 iterations are used to burn in the ensemble. We list the fitting results of the derived model parameters in Table 2, while the detailed fittings to the multi-band lightcurves for each event are shown in the Appendix A. Generally, the FBOT lightcurves can be well fitted by the magnetar engine model with high quality. For example, we present the posteriors of the fitting parameters for DES16C3gin in Figure 5.

3. RESULTS AND DISCUSSIONS

3.1. Properties of FBOTs and their possible origins

The most important outputs of the lightcurve modeling are the ejecta mass M_{ej} , initial spin period P_i , and magnetic field strength B_p . We plot M_{ej} vs. P_i and P_i vs. B_p in Figures 1 and 2, respectively. The ejecta masses for most of FBOTs we collected are in the range of $\sim 0.002 - 1 M_\odot$ with a median value of $\sim 0.11 M_\odot$. For the magnetars, the initial spin periods are centered at $\sim 9.1^{+9.3}_{-4.4}$ ms. The magnetic field strengths, in which the median value is $\sim 25 B_c$, have a wide distribution mostly between $\sim B_c$ and $\sim 200 B_c$. Here, $B_c = m_e^2 c^3 / (q \hbar) = 4.4 \times 10^{13}$ G represents the Landau critical magnetic field defined by electron mass m_e , electron charge q and reduced Planck constant \hbar .

Corresponding to our sample selection criterion as $t_{\text{rise}} \lesssim 10$ d, the upper limit of the ejecta masses of FBOTs can be set to be around $1 M_\odot$, which hints that FBOTs could have the following types of origins with the formation of a rapidly rotating magnetar: (I) BNS mergers to produce massive NS remnants (i.e., the mergernova model; Yu et al. 2013), (II) mergers of a NS and a WD (Zenati et al. 2019), (III) AICs of WDs, including both single- and double-degenerate cases² (Yu et al. 2019a,b), and (IV) SN explosions of ultra-stripped stars (i.e., ultra-stripped SNe; e.g., Tauris et al. 2015; Hotokezaka et al. 2017; Sawada et al. 2022). For Case I, since the derived masses here are generally higher than the masses that can be produced by the BNS mergers (e.g., Radice et al. 2018), the mergernova model could be ruled out for most FBOTs. Nevertheless, the model could still account for some special sources such as PS1-12bb, which have the fastest evolution and relatively low luminosities that are consistent with the prediction of the mergernova model. Furthermore, if a larger opacity is taken into account which can be caused by lanthanides, then more samples could be classified to the mergernova candidates as their ejecta masses become smaller than $\lesssim 0.01 M_\odot$. In any case, the rel-

atively low event rate of the BNS mergers definitely makes them can only account for a very small fraction of the observed FBOTs. Alternatively, in comparison, the relatively wide range of the ejecta masses of FBOTs most favors the ultra-stripped SN model in close binaries, although it is unclear how newborn NSs formed via this channel can have an initial spin period as high as $P_i \sim 2 - 40$ ms. We infer that the compact companion in a close binary can increase the angular momentum of the ultra-stripped star by the tidal torque, possibly resulting in the rapid rotation of the NS. In addition, for the FBOTs with ejecta masses around $\sim 0.1 M_\odot$, the WD-related models still cannot be ruled out, which have some advantages in explaining the multi-wavelength features of some FBOTs.

3.2. Connection with SLSNe and SNe Ic-BL

It has been widely suggested that SLSNe and SNe Ic-BL associated/unassociated with IGRBs, at least a good fraction of them, are also driven by millisecond magnetars (e.g., Kasen & Bildsten 2010; Lü & Zhang 2014; Mazzali et al. 2014; Metzger et al. 2015; Kashiyama et al. 2016; Yu et al. 2017; Liu et al. 2017; Nicholl et al. 2017; Lü et al. 2018). Therefore, it is necessary and interesting to investigate the possible connection and differences between FBOTs and these explosion phenomena, as did in (e.g., Milisavljevic et al. 2013; Yu et al. 2017; Margutti et al. 2019; Pian et al. 2020) for connecting normal SNe Ib/c, SLSNe, and IGRBs. For comparison, we display FBOTs along with SLSNe, GRB-SNe and normal SNe Ic-BL in the M_{ej} vs. P_i space in Figure 1, and in the P_i vs. B_p space in Figure 2. The P_i values for GRB-SNe and normal SNe Ic-BL are collected from Lyman et al. (2016); Lü et al. (2018); Taddia et al. (2019) by assuming that the kinetic energy of the ejecta is derived from the rotational energy of the magnetar.

As shown in Figure 1, the combination of the four different types of transients shows a clear universal correlation between ejecta mass and initial spin period as

$$P_i \propto M_{\text{ej}}^{-0.41}, \quad (4)$$

with a Pearson correlation coefficient $\rho = -0.84$, which is well consistent with the results discovered by Yu et al. (2017) for the SLSN sample only. This anti-correlation strongly indicates that these explosion phenomena may share a common origin. It can be also found that the clearest criterion defining FBOTs could be their small ejecta masses, which generally corresponds to relatively large initial spin periods because of the strong anti-correlation. Therefore, on the one hand, FBOTs very likely originate from stellar collapses, just having a progenitor much lighter and much more stripped than

² Binary NS or WD mergers and WD AICs can occur in active galactic nucleus accretion disks to drive bright magnetar-powered explosions (Zhu et al. 2021a,b).

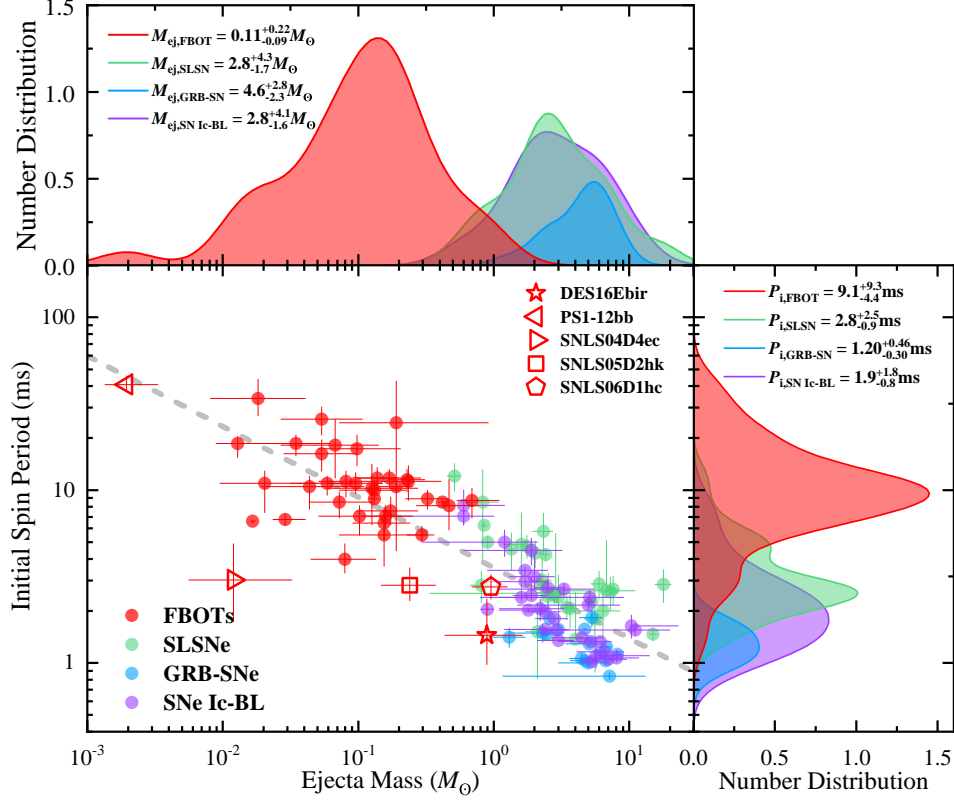


Figure 1. Relationship between ejecta masses of FBOTs and initial spin periods of FBOT magnetars (red points). The green, blue, and violet points correspond to the cases of SLSNe (Yu et al. 2017), GRB-SNe (Lü et al. 2018), and SNe Ic-BL (Lyman et al. 2016; Taddia et al. 2019), respectively. The best-fitting log-linear relation $P_i \propto M_{ej}^{-0.41}$ is shown by the dashed line. The top and right panels display the number distributions of ejecta masses and initial NS periods, derived by the method of the kernel density estimation, for these four types of explosions.

those of SLSNe and SNe Ic-BL. On the other hand, the $M_{ej} - P_i$ anti-correlation indicates that more massive progenitors have larger angular momenta. In Section 3.1, we suspect that the FBOT progenitors could be ultra-stripped stars in close binary systems, which can be spun up by their compact companions. Following this consideration, the $M_{ej} - P_i$ anti-correlation could be a natural result of the interaction between the progenitor and the compact companion (see also Blanchard et al. 2020; Fuller & Lu 2022, Hu et al. 2022, in Preparation). If this hypothesis is true, then it is expected that the progenitors of SLSNe and SNe Ic-BL can also be substantially influenced by a compact companion.

Yu et al. (2017) have found that the primary difference between SLSNe and lGRBs could be the magnetic field strengths of their magnetar engines. Specifically, SLSNe have $B_c \lesssim B_p \lesssim 10B_c$, while lGRBs have $B_p \gtrsim 10B_c$. Therefore, in Yu et al. (2017), it was suspected that the ultra-high magnetic fields can play a crucial role in launching a relativistic jet to produce GRB emission. Here, it is however found that the surface magnetic fields of more than half FBOTs can be higher than $10B_c$, but no GRB has been detected to be associated with

FBOTs. One possibility is that the GRB emission associating these FBOTs is highly beamed and the emission beam largely deviates from the line of sight. This, however, is disfavored by the difference between the event rate density of FBOTs and lGRBs. Therefore, a more promising explanation is that these FBOT magnetars intrinsically cannot produce GRB emission, even though their magnetic fields satisfy $B_p > 10B_c$. The probable reason is that the FBOT magnetars rotate too slowly to provide sufficiently large energy for a relativistic jet. Additionally, in view of the small masses of the FBOT ejecta, the possible fallback accretion onto the magnetar is also potentially weak and thus cannot help to launch the jet.

Finally, in view of the significant similarity between FBOTs and SLSNe, it would be reasonable to regard them as an unified phenomenon with different progenitor masses. From this view, the separation between FBOTs and SLSNe is empirical but does not imply fundamentally different physics. For example, the FBOTs, DES16E1bir ($M_{ej} \sim 0.9 M_\odot$) and SNLS06D1hc ($M_{ej} \sim 1 M_\odot$), in our sample could in fact be classified into SLSNe. In any case, by combining with the FBOT and

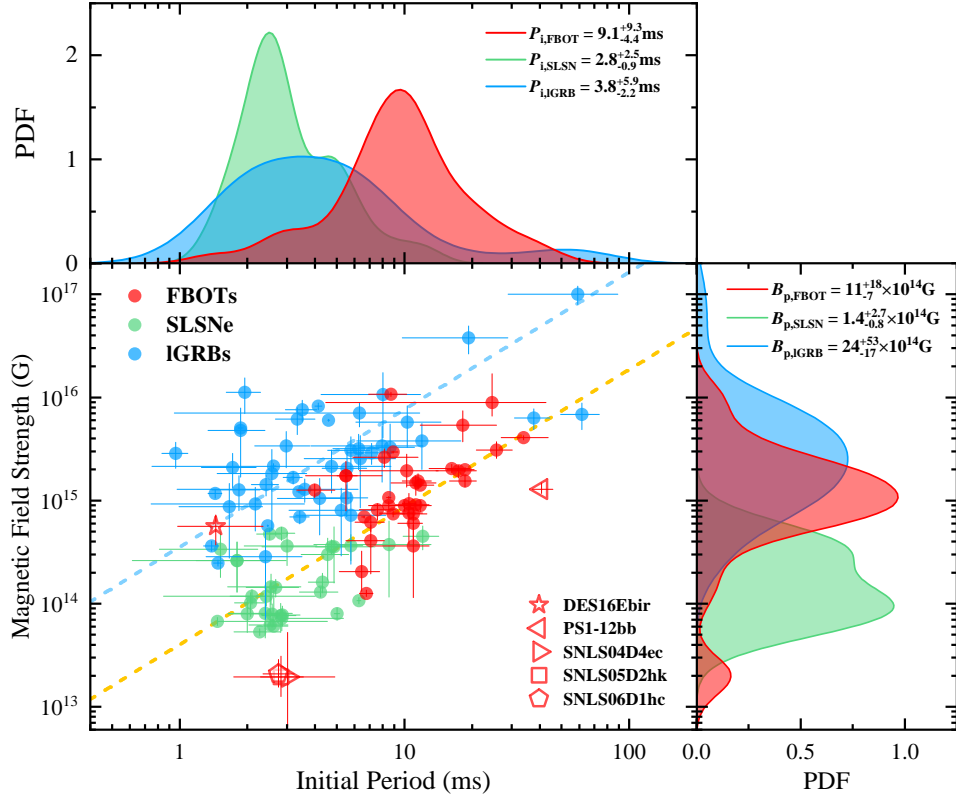


Figure 2. Magnetic field strengths of FBOT magnetars against the initial spin periods (red points). Magnetar parameters for SLSN (green points) and IGRB (blue points) are collected from Yu et al. (2017) and Lü & Zhang (2014), respectively. Orange and blue dashed lines represent the parallel fitting $P_i - B_p$ anti-correlations of the magnetars for the FBOTs plus SLSNe and IGRBs, respectively. The probability density functions of the magnetic field strength and initial spin period distributions for these three types of explosions are displayed in the top and right panels, respectively.

SLSN data, we can find a weak correlation between P_i and B_p , as presented in Figure 2. Such a correlation could also exist in the IGRB data, but with a shift in B_p . This indicates that GRB magnetars have magnetic fields statistically higher than those of SLSNe and FBOTs for the same initial spin period P_i .

3.3. Shape of Lightcurves

According to the parameter values constrained from the fittings, we can calculate the peak absolute magnitude (or peak luminosity), the rise and decline timescales above half-maximum luminosity of the FBOTs, and their 1σ uncertainties, which are also listed in Table 2. These parameters determine the basic shape of the lightcurves of the transients and can be measured directly from observational data, which therefore are very useful for classifying the transients. As presented in the left panel of Figure 3, it seems reasonable to set the boundary between FBOTs and SLSNe at $t_{\text{rise}} \sim 10$ d where the data are relatively sparse. So we adopt it as a sample selection criterion. Strictly speaking, it cannot be ruled out that the ambiguous gap between FBOTs and SLSNe could just be a result of selection effects

and the distribution between these two phenomenological types of explosion phenomena could in fact be intrinsically continuous.

Generally speaking, FBOTs together with SLSNe can be separated from SNe Ic-BL including GRB-SNe by the separation line

$$M_{\text{peak}} = \begin{cases} a_1 \tilde{t}_{\text{rise}} - b_1 \log_{10} \tilde{t}_{\text{rise}} - c_1, & \text{for } \tilde{t}_{\text{rise}} \lesssim 30, \\ a_2 \tilde{t}_{\text{rise}} - b_2 \log_{10} \tilde{t}_{\text{rise}} - c_2, & \text{for } \tilde{t}_{\text{rise}} \gtrsim 30, \end{cases} \quad (5)$$

which corresponds to a nickel mass $M_{\text{Ni}} = 0.3 M_{\text{ej}}$, where $\tilde{t}_{\text{rise}} = t_{\text{rise}}/\text{d}$ and the numerical coefficients read $a_1 = 0.083$, $b_1 = 5.3$, $c_1 = 14.94$, $a_2 = 0.0089$, $b_2 = 5.2$, and $c_2 = 12.63$. This separation line is plotted using the $M_{\text{ej}} - E_K$ relationship derived from the $M_{\text{ej}} - P_i$ relationship, i.e., Equation (4), by assuming that all the kinetic energy of the ejecta comes from the rotational energy of the magnetar. It is commonly believed that the mass of the ^{56}Ni synthesized during core-collapse SNe is very difficult to reach a few tens percent of the total mass of the SN ejecta (e.g., Suwa et al. 2015; Saito et al. 2022). Based on radiation transport calculations, Ertl

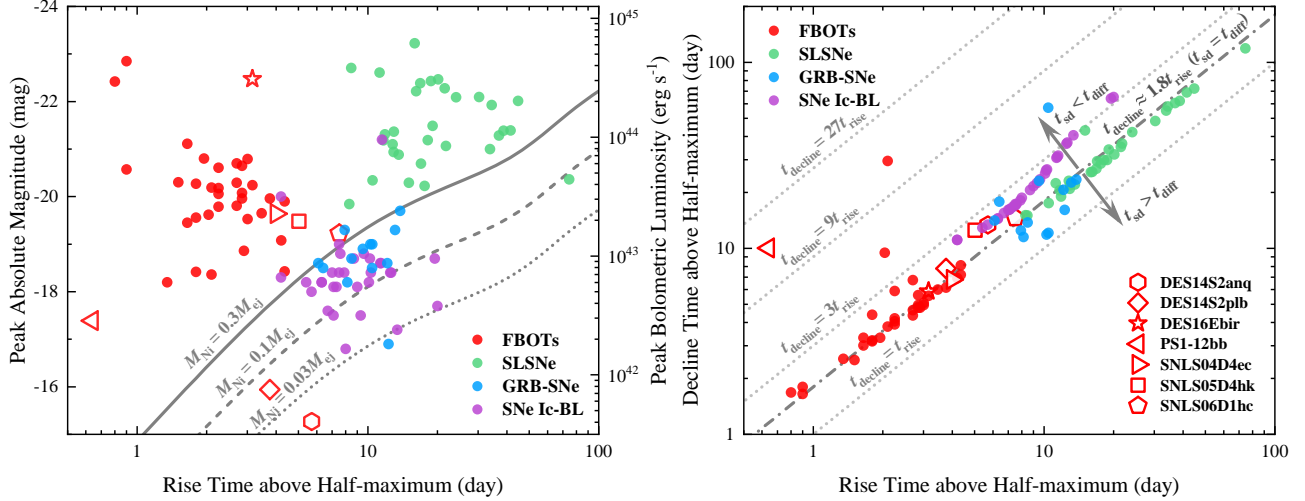


Figure 3. Left panel: peak absolute magnitudes against the rise times for FBOTs (red points), SLSNe (green points), GRB-SNe (blue points) and SNe Ic-BL (purple points). The solid, dashed and dotted lines are the conditions of $M_{\text{Ni}} = 0.3M_{\text{ej}}$, $0.1M_{\text{ej}}$ and $0.03M_{\text{ej}}$, respectively. Right panel: decline times against the rise times for these four types of explosions. The dashed-dotted line, i.e., $t_{\text{decl}} \approx 1.8t_{\text{rise}}$, corresponds to $t_{\text{sd}} = t_{\text{diff}}$. The dotted lines represent the different relationships between these two timescales as labeled.

et al. (2020) found that current models employing standard assumptions of the explosions and nucleosynthesis predicts radioactive decay powered light curves that are less luminous than commonly observed SNe Ib and Ic. So, both FBOTs and SLSNe of magnitudes above Equation (5) definitely cannot be primarily powered by radioactive decay of ^{56}Ni and an engine power is required. Nevertheless, some outliers still exist in our sample, e.g., DES14S2anq and DES14S2plb. In comparison, the peak luminosity of SNe Ic-BL is relatively lower, which reduces the energy requirement and, in principle, makes the radioactive power model available. Nevertheless, by considering of the continuous transition between different phenomena, it could still be nature to suggest that the emission of a fraction of SNe Ic-BL including GRB-SNe is also partly powered by the magnetar engine, although the majority of the spin-down energy of the magnetar has been converted to the kinetic energy of the SN ejecta (e.g., Lin et al. 2021; Zhang et al. 2022).

As analyzed in Yu et al. (2015, 2017), the emission fraction of the spin-down energy is primarily determined by the relationship between the timescales of t_{sd} and t_{diff} , which can be basically reflected by the ratio of the lightcurve rise to the decline times. As shown in the right panel of Figure 3, the FBOT and SLSN data can be well fitted by the line of $t_{\text{decl}} \approx 1.8t_{\text{rise}}$, which corresponds to $t_{\text{sd}} = t_{\text{diff}}$. This is a reason why we can regard FBOTs and SLSNe as an unified phenomenon. In comparison, the SNe Ic-BL data are obviously in the $t_{\text{sd}} < t_{\text{diff}}$ region, as expected. For GRB-SNe, although they are usually classified as SNe Ic-BL, their distribu-

tion in the $t_{\text{rise}} - t_{\text{decl}}$ plane is actually more diffusive than normal SNe Ic-BL.

4. CONCLUSION

In this paper, we perform a systematic analysis of multi-band lightcurves of 40 FBOTs using the magnetar engine model and most samples are fitted with high quality. Then, the explosion and magnetar parameters are well constrained. It is found that the median values with 1σ deviation of ejecta mass and initial spin period of the FBOT magnetars are $M_{\text{ej}} = 0.11_{-0.09}^{+0.22} M_{\odot}$ and $P_1 = 9.1_{-4.4}^{+9.3}$ ms. The magnetic field strengths B_p are mostly between $\sim B_c$ and $\sim 200B_c$ with a median value of $\sim 25B_c$. Here, please keep in mind that the value of M_{ej} is somewhat dependent on the adoption of the ejecta velocity. If FBOT explosions can be initially as explosive as and even more explosive than normal SNe Ib/c, the value of M_{ej} would be systematically increased by a factor of ~ 2 so that an appropriate diffusion timescale can be kept.

In view of that the star-formation rates and metallicities of the FBOT hosts are consistent with those of SLSNe and SNe Ic-BL including GRB-SNe (Wiseman et al. 2020), we compare the derived parameters of the FBOTs with the other types of extreme stripped-envelope explosions which are potentially driven by magnetar engines too. Consequently, we find a strong continuous anti-correlation between M_{ej} and P_1 for FBOTs, SLSNe, GRB-SNe and SNe Ic-BL as $P_1 \propto M_{\text{ej}}^{-0.41}$. A clear criterion to define FBOTs is their small ejecta masses, with an upper limit of $\sim 1 M_{\odot}$, which is around the lower limit of the masses of other explosion phe-

nomena. Furthermore, the magnetic field strengths of the FBOT magnetars span from $\sim B_c \lesssim B_p \lesssim 10B_c$ for SLSN magnetars to $B_p \gtrsim 10B_c$ for IGRB magnetars. These connections indicate that most FBOTs may share a common origin with SLSNe, IGRBs and normal SNe Ic-BL. Since the progenitors of FBOTs likely have low masses, we suspect that most FBOTs originate from the collapse of ultra-stripped stars in close binary systems. However, mergernovae and WD-related models are still not ruled out, which could give nature explanations for some special outlier samples.

With the distributions of t_{rise} vs. M_{peak} for these different types of explosions, we know that the FBOT and SLSN data can be separated by a criterion of $t_{\text{rise}} \sim 10$ d, while FBOTs together with SLSNe can be separated

from GRB-SNe and normal SNe Ic-BL by the line corresponding to $M_{\text{Ni}} = 0.3M_{\text{ej}}$. These criteria can be used to classify FBOTs, SLSNe and SNe Ic-BL in observation.

ACKNOWLEDGMENTS

We thank the anonymous reviewer for helpful comments and feedback. We thank Sheng Yang, Ying Qin, Rui-Chong Hu, and Noam Soker for helpful comments, H-J. Lü, M. R. Drout and M. Pursiainen for sharing their data. This work is supported by the National SKA program of China (2020SKA0120300), the National Key R&D Program of China (2021YFA0718500), and the National Natural Science Foundation of China (Grant No. 11833003).

APPENDIX

A. FBOT SAMPLES AND FITTING RESULTS

The observed data and fitting lightcurves for the FBOTs collected in our sample are presented in Figure 4.

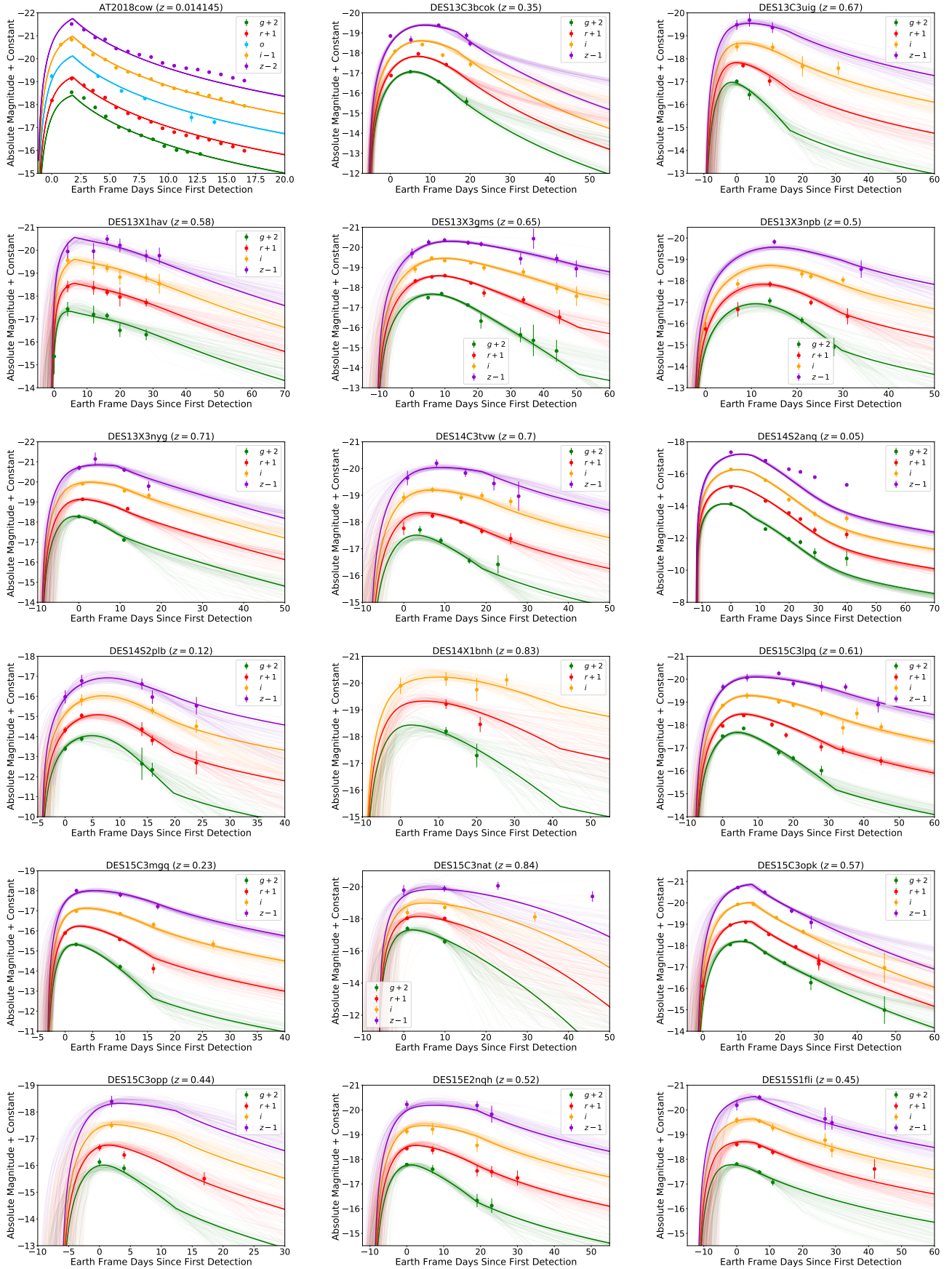


Figure 4. Multi-band observations and fittings for the FBOTs by the magnetar-powered model.

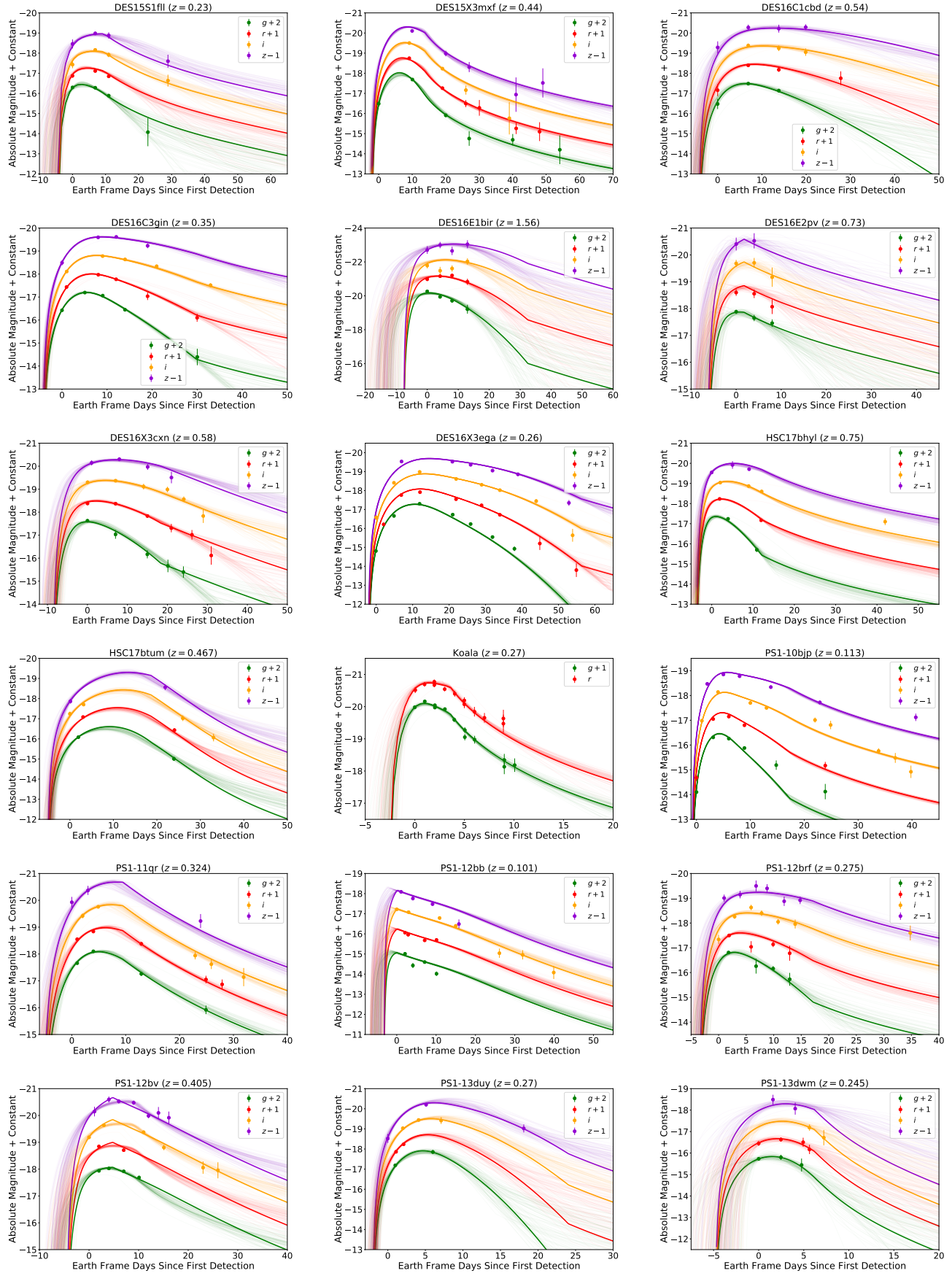


Figure 4. (Continued.)

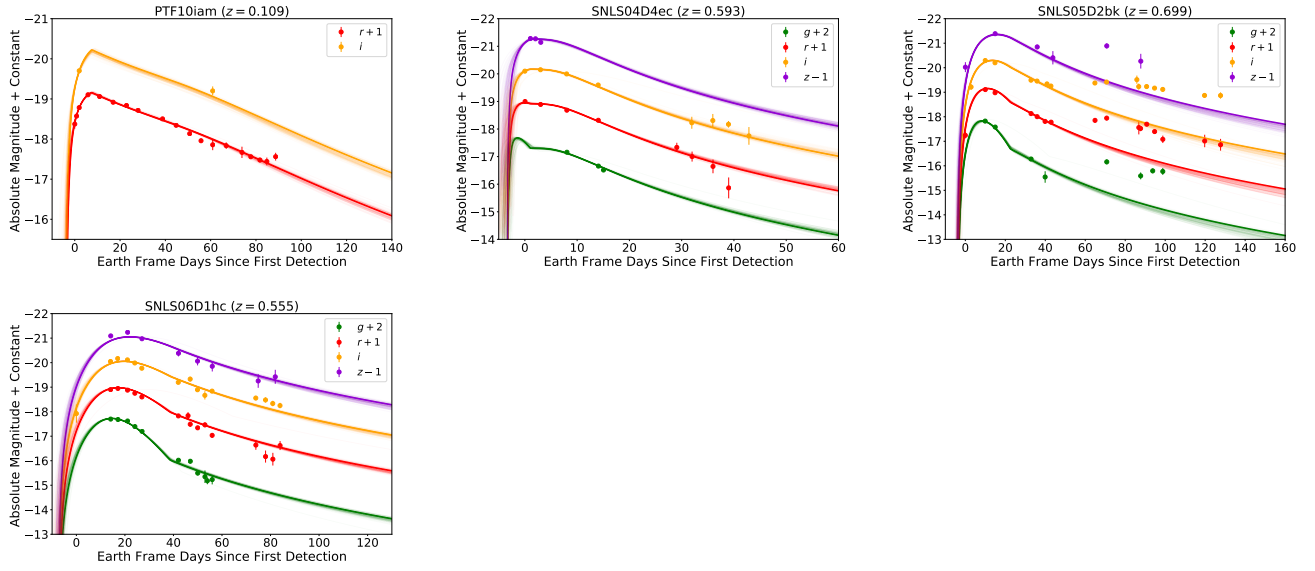


Figure 4. (Continued.)

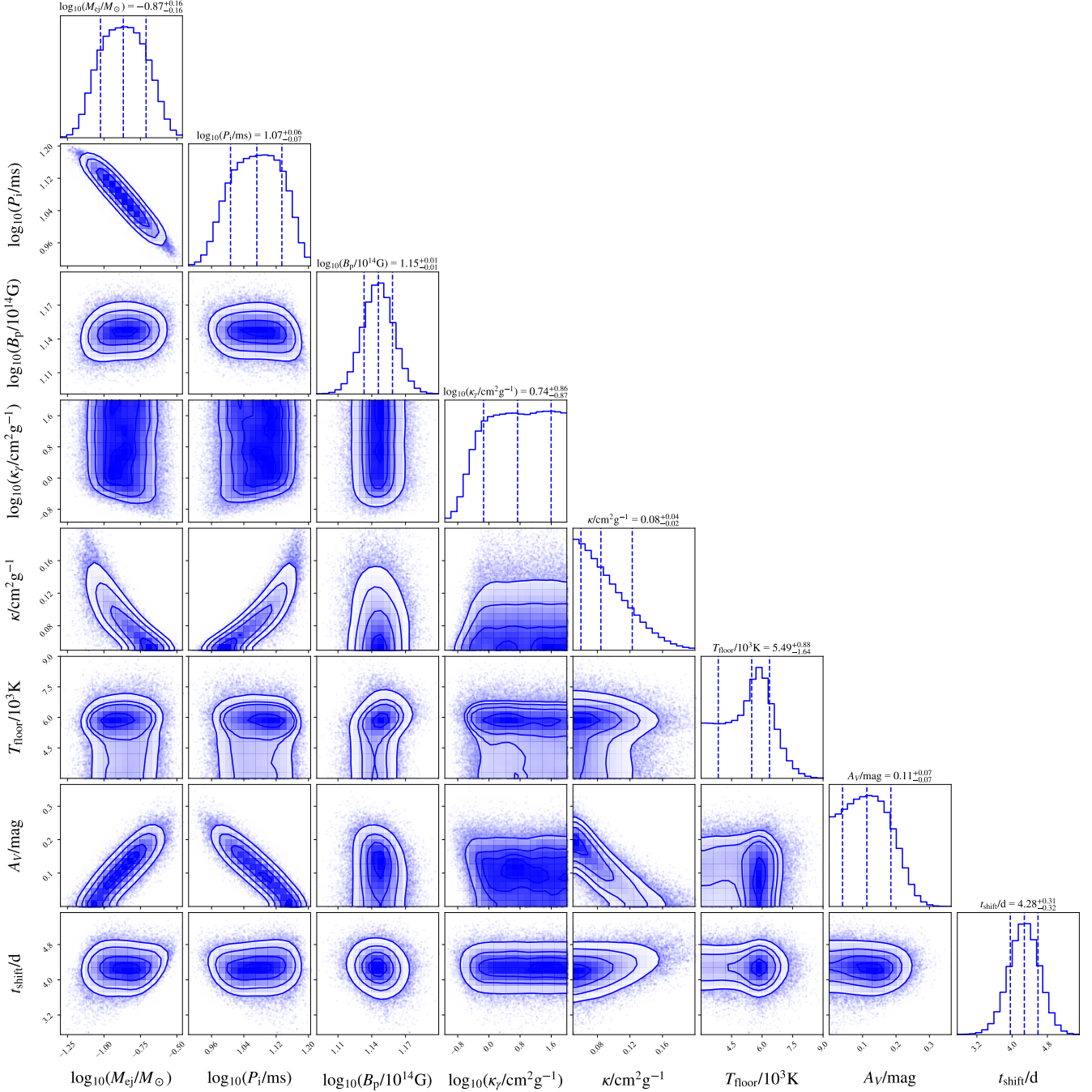


Figure 5. Posteriors for magnetar model fit to DES16C3gin. Medians and 1 σ ranges are labeled.

Table 2. The lightcurve properties and the fitting results of the derived parameters for the collected FBOTs

FBOT	M_{peak}	t_{rise}	t_{decl}	$\log_{10} M_{\text{ej},\odot}$	$\log_{10} P_{1,-3}$	$\log_{10} B_{\text{p},14}$	$\log_{10} \kappa_{\gamma}$	κ	$T_{\text{floor},3}$	A_V
AT2018cow	$-22.42^{+0.03}_{-0.04}$	$0.80^{+0.04}_{-0.00}$	$1.68^{+0.04}_{-0.04}$	$-1.78^{+0.02}_{-0.01}$	$0.82^{+0.00}_{-0.01}$	$0.84^{+0.01}_{-0.01}$	$1.83^{+0.12}_{-0.14}$	$0.19^{+0.01}_{-0.01}$	$24.58^{+0.27}_{-0.16}$	$0.50^{+0.00}_{-0.00}$
DES13C3bcok	$-19.53^{+0.14}_{-0.13}$	$3.01^{+0.30}_{-0.15}$	$4.96^{+0.45}_{-0.30}$	$-0.64^{+0.13}_{-0.14}$	$1.06^{+0.07}_{-0.07}$	$1.19^{+0.07}_{-0.08}$	$-0.7^{+1.8}_{-1.2}$	$0.06^{+0.02}_{-0.01}$	$10.5^{+2.0}_{-1.1}$	$0.03^{+0.04}_{-0.02}$
DES13C3uig*	$-19.45^{+0.33}_{-0.37}$	$1.65^{+0.30}_{-0.45}$	$3.31^{+0.60}_{-0.75}$	$-1.46^{+0.25}_{-0.26}$	$1.27^{+0.05}_{-0.07}$	$1.19^{+0.06}_{-0.06}$	$1.07^{+0.64}_{-0.74}$	$0.10^{+0.06}_{-0.04}$	$7.9^{+1.2}_{-1.3}$	$0.15^{+0.17}_{-0.11}$
DES13X1hav*	$-19.62^{+0.41}_{-0.36}$	$2.0^{+5.2}_{-0.7}$	$9.5^{+5.3}_{-3.5}$	$-1.69^{+0.38}_{-0.33}$	$1.04^{+0.07}_{-0.17}$	$0.56^{+0.20}_{-0.50}$	$1.22^{+0.54}_{-0.78}$	$0.13^{+0.05}_{-0.05}$	$12.2^{+1.7}_{-1.4}$	$0.29^{+0.15}_{-0.18}$
DES13X3gms	$-19.90^{+0.23}_{-0.26}$	$4.36^{+0.60}_{-0.45}$	$7.21^{+0.90}_{-0.75}$	$-0.49^{+0.16}_{-0.16}$	$0.95^{+0.05}_{-0.06}$	$0.87^{+0.03}_{-0.03}$	$0.5^{+1.0}_{-1.1}$	$0.08^{+0.04}_{-0.02}$	$6.1^{+1.9}_{-2.1}$	$0.14^{+0.11}_{-0.09}$
DES13X3npb	$-19.08^{+0.26}_{-0.29}$	$4.21^{+0.45}_{-0.45}$	$6.91^{+0.90}_{-0.75}$	$-0.63^{+0.24}_{-0.20}$	$1.05^{+0.09}_{-0.11}$	$1.17^{+0.07}_{-0.12}$	$0.1^{+1.3}_{-1.2}$	$0.12^{+0.05}_{-0.05}$	$6.5^{+3.1}_{-2.4}$	$0.23^{+0.17}_{-0.15}$
DES13X3nyg*	$-21.11^{+0.35}_{-0.34}$	$1.65^{+0.45}_{-0.30}$	$3.01^{+0.60}_{-0.45}$	$-1.14^{+0.25}_{-0.22}$	$0.93^{+0.06}_{-0.09}$	$0.95^{+0.04}_{-0.04}$	$0.82^{+0.78}_{-0.86}$	$0.10^{+0.06}_{-0.03}$	$10.7^{+1.5}_{-4.0}$	$0.19^{+0.14}_{-0.13}$
DES14C3tvw	$-19.65^{+0.27}_{-0.30}$	$3.46^{+0.90}_{-0.75}$	$6.0^{+1.5}_{-1.1}$	$-0.77^{+0.23}_{-0.24}$	$1.07^{+0.05}_{-0.06}$	$0.95^{+0.05}_{-0.06}$	$0.5^{+1.0}_{-1.0}$	$0.08^{+0.05}_{-0.02}$	$8.7^{+2.4}_{-3.8}$	$0.10^{+0.13}_{-0.07}$
DES14S2anq*	$-15.27^{+0.04}_{-0.06}$	$5.71^{+0.15}_{-0.15}$	$13.37^{+0.45}_{-0.30}$	$-0.16^{+0.20}_{-0.11}$	$0.94^{+0.07}_{-0.10}$	$2.03^{+0.02}_{-0.02}$	$0.4^{+1.1}_{-1.2}$	$0.15^{+0.04}_{-0.05}$	$5.63^{+0.29}_{-0.24}$	$0.03^{+0.05}_{-0.02}$
DES14S2plb	$-15.94^{+0.83}_{-0.54}$	$3.76^{+0.60}_{-0.60}$	$7.8^{+3.0}_{-2.1}$	$-0.72^{+0.68}_{-0.42}$	$1.39^{+0.24}_{-0.74}$	$1.95^{+0.28}_{-0.13}$	$0.2^{+1.3}_{-1.2}$	$0.13^{+0.05}_{-0.05}$	$5.7^{+1.5}_{-1.3}$	$0.35^{+0.12}_{-0.22}$
DES14X1bnh*	$-20.70^{+0.44}_{-0.49}$	$2.7^{+1.1}_{-0.8}$	$6.8^{+5.4}_{-2.1}$	$-0.99^{+0.31}_{-0.30}$	$0.85^{+0.06}_{-0.11}$	$0.61^{+0.15}_{-0.32}$	$0.85^{+0.81}_{-0.96}$	$0.11^{+0.06}_{-0.04}$	$8.6^{+5.5}_{-3.7}$	$0.25^{+0.16}_{-0.17}$
DES15C3lpq	$-20.08^{+0.15}_{-0.14}$	$2.85^{+0.45}_{-0.30}$	$4.96^{+0.60}_{-0.60}$	$-0.72^{+0.12}_{-0.13}$	$1.02^{+0.03}_{-0.03}$	$0.97^{+0.02}_{-0.02}$	$0.66^{+0.89}_{-0.83}$	$0.06^{+0.01}_{-0.01}$	$7.66^{+0.80}_{-0.76}$	$0.03^{+0.04}_{-0.02}$
DES15C3mgq*	$-18.20^{+0.29}_{-0.36}$	$1.35^{+0.75}_{-0.45}$	$2.55^{+0.90}_{-0.60}$	$-1.74^{+0.35}_{-0.35}$	$1.53^{+0.11}_{-0.10}$	$1.61^{+0.02}_{-0.02}$	$1.07^{+0.63}_{-0.75}$	$0.14^{+0.04}_{-0.05}$	$5.23^{+0.94}_{-0.70}$	$0.39^{+0.08}_{-0.17}$
DES15C3nat*	$-19.79^{+0.35}_{-0.39}$	$2.25^{+0.60}_{-0.60}$	$3.9^{+1.1}_{-0.9}$	$-0.90^{+0.34}_{-0.32}$	$1.01^{+0.14}_{-0.21}$	$1.29^{+0.16}_{-0.16}$	$0.3^{+1.2}_{-1.4}$	$0.09^{+0.06}_{-0.03}$	$6.1^{+2.6}_{-2.2}$	$0.12^{+0.15}_{-0.09}$
DES15C3opk	$-20.79^{+0.25}_{-0.35}$	$3.01^{+0.60}_{-0.45}$	$5.1^{+1.2}_{-0.6}$	$-0.80^{+0.20}_{-0.17}$	$0.85^{+0.06}_{-0.07}$	$0.79^{+0.07}_{-0.09}$	$-0.4^{+1.4}_{-0.5}$	$0.12^{+0.05}_{-0.05}$	$17.5^{+1.3}_{-1.3}$	$0.30^{+0.10}_{-0.11}$
DES15C3opp*	$-18.36^{+0.33}_{-0.39}$	$2.10^{+0.75}_{-0.60}$	$3.8^{+1.1}_{-1.1}$	$-1.27^{+0.30}_{-0.30}$	$1.41^{+0.07}_{-0.09}$	$1.49^{+0.08}_{-0.08}$	$0.4^{+1.1}_{-1.1}$	$0.08^{+0.05}_{-0.02}$	$7.1^{+2.0}_{-2.7}$	$0.09^{+0.13}_{-0.06}$
DES15E2nqh*	$-20.29^{+0.28}_{-0.30}$	$2.70^{+0.60}_{-0.75}$	$4.66^{+0.90}_{-0.90}$	$-0.88^{+0.23}_{-0.26}$	$1.00^{+0.06}_{-0.07}$	$0.95^{+0.04}_{-0.05}$	$0.68^{+0.91}_{-0.96}$	$0.08^{+0.05}_{-0.02}$	$8.3^{+1.2}_{-2.4}$	$0.09^{+0.12}_{-0.07}$
DES15S1ffi*	$-20.06^{+0.29}_{-0.39}$	$2.25^{+0.60}_{-0.60}$	$5.9^{+2.4}_{-1.5}$	$-1.23^{+0.24}_{-0.27}$	$1.04^{+0.04}_{-0.07}$	$0.78^{+0.09}_{-0.15}$	$1.23^{+0.53}_{-0.68}$	$0.12^{+0.05}_{-0.05}$	$11.0^{+2.3}_{-2.7}$	$0.17^{+0.18}_{-0.12}$
DES15S1flf*	$-18.86^{+0.37}_{-0.45}$	$2.9^{+1.1}_{-0.9}$	$4.8^{+1.8}_{-1.4}$	$-1.01^{+0.32}_{-0.28}$	$1.24^{+0.08}_{-0.10}$	$1.29^{+0.05}_{-0.07}$	$0.5^{+1.1}_{-1.0}$	$0.10^{+0.05}_{-0.03}$	$7.1^{+2.7}_{-2.5}$	$0.09^{+0.10}_{-0.06}$
DES15X3mxf	$-20.61^{+0.22}_{-0.18}$	$2.25^{+0.30}_{-0.15}$	$4.06^{+0.45}_{-0.45}$	$-0.53^{+0.09}_{-0.11}$	$0.74^{+0.05}_{-0.04}$	$1.24^{+0.02}_{-0.02}$	$0.69^{+0.90}_{-0.93}$	$0.06^{+0.03}_{-0.01}$	$11.29^{+0.81}_{-0.66}$	$0.03^{+0.05}_{-0.02}$
DES16C1cbd	$-19.96^{+0.31}_{-0.32}$	$2.85^{+0.60}_{-0.60}$	$5.6^{+1.1}_{-1.1}$	$-1.02^{+0.20}_{-0.21}$	$1.04^{+0.06}_{-0.06}$	$0.87^{+0.06}_{-0.06}$	$0.70^{+0.89}_{-0.93}$	$0.12^{+0.05}_{-0.05}$	$7.2^{+2.4}_{-2.9}$	$0.34^{+0.11}_{-0.16}$
DES16C3gin	$-19.81^{+0.26}_{-0.25}$	$2.70^{+0.15}_{-0.30}$	$4.36^{+0.30}_{-0.30}$	$-0.86^{+0.16}_{-0.15}$	$1.07^{+0.06}_{-0.06}$	$1.15^{+0.01}_{-0.01}$	$0.73^{+0.87}_{-0.86}$	$0.08^{+0.04}_{-0.02}$	$5.5^{+0.9}_{-1.7}$	$0.11^{+0.07}_{-0.07}$
DES16E1bir*	$-22.47^{+0.15}_{-0.29}$	$3.16^{+0.45}_{-0.45}$	$5.86^{+0.75}_{-0.75}$	$-0.05^{+0.26}_{-0.31}$	$0.16^{+0.06}_{-0.17}$	$0.75^{+0.11}_{-0.18}$	$0.4^{+1.1}_{-1.1}$	$0.11^{+0.05}_{-0.04}$	$9.8^{+4.7}_{-4.8}$	$0.10^{+0.14}_{-0.07}$
DES16E2pv*	$-20.27^{+0.34}_{-0.42}$	$1.80^{+0.63}_{-0.60}$	$4.4^{+3.0}_{-1.2}$	$-1.36^{+0.40}_{-0.35}$	$1.02^{+0.06}_{-0.13}$	$0.88^{+0.19}_{-0.30}$	$0.7^{+0.9}_{-1.1}$	$0.11^{+0.06}_{-0.05}$	$16.7^{+2.3}_{-5.6}$	$0.18^{+0.17}_{-0.12}$
DES16X3cxn*	$-20.18^{+0.34}_{-0.42}$	$2.25^{+0.60}_{-0.45}$	$4.21^{+0.90}_{-0.75}$	$-1.09^{+0.20}_{-0.20}$	$1.05^{+0.06}_{-0.09}$	$0.96^{+0.03}_{-0.03}$	$0.69^{+0.88}_{-0.78}$	$0.10^{+0.06}_{-0.04}$	$5.4^{+2.3}_{-1.6}$	$0.24^{+0.15}_{-0.15}$
DES16X3ega	$-19.96^{+0.04}_{-0.03}$	$3.76^{+0.00}_{-0.15}$	$6.16^{+0.00}_{-0.15}$	$-0.38^{+0.03}_{-0.03}$	$0.93^{+0.01}_{-0.01}$	$1.03^{+0.01}_{-0.01}$	$-1.20^{+0.06}_{-0.05}$	$0.05^{+0.00}_{-0.00}$	$3.45^{+0.32}_{-0.30}$	$0.16^{+0.03}_{-0.03}$
HSC17bhy1*	$-20.57^{+0.21}_{-0.28}$	$0.90^{+0.30}_{-0.15}$	$1.80^{+0.45}_{-0.30}$	$-1.89^{+0.27}_{-0.16}$	$1.27^{+0.04}_{-0.08}$	$1.30^{+0.02}_{-0.02}$	$1.57^{+0.30}_{-0.40}$	$0.14^{+0.06}_{-0.04}$	$8.13^{+0.60}_{-0.67}$	$0.08^{+0.15}_{-0.06}$
HSC17btum*	$-18.43^{+0.21}_{-0.27}$	$4.36^{+0.30}_{-0.30}$	$8.11^{+0.75}_{-0.75}$	$-0.33^{+0.22}_{-0.24}$	$0.91^{+0.15}_{-0.14}$	$1.42^{+0.08}_{-0.10}$	$-0.6^{+1.7}_{-1.1}$	$0.10^{+0.06}_{-0.04}$	$10.6^{+1.0}_{-0.8}$	$0.10^{+0.09}_{-0.06}$
Koala	$-22.85^{+0.32}_{-0.35}$	$0.90^{+0.30}_{-0.15}$	$1.65^{+0.30}_{-0.45}$	$-1.10^{+0.23}_{-0.25}$	$0.60^{+0.09}_{-0.08}$	$1.10^{+0.06}_{-0.07}$	$0.99^{+0.69}_{-0.73}$	$0.09^{+0.05}_{-0.03}$	$15.7^{+1.7}_{-1.6}$	$0.04^{+0.06}_{-0.03}$
PS1-10bjp	$-20.30^{+0.04}_{-0.04}$	$1.51^{+0.00}_{-0.10}$	$2.51^{+0.00}_{-0.10}$	$-0.88^{+0.03}_{-0.04}$	$0.95^{+0.02}_{-0.01}$	$1.47^{+0.01}_{-0.01}$	$1.03^{+0.65}_{-0.65}$	$0.05^{+0.00}_{-0.00}$	$5.44^{+0.22}_{-0.21}$	$0.48^{+0.01}_{-0.02}$
PS1-11qr	$-20.24^{+0.26}_{-0.32}$	$3.16^{+0.60}_{-0.45}$	$5.56^{+0.75}_{-0.60}$	$-0.81^{+0.19}_{-0.23}$	$0.81^{+0.08}_{-0.10}$	$0.31^{+0.20}_{-0.19}$	$-1.44^{+0.51}_{-0.38}$	$0.13^{+0.05}_{-0.05}$	$13.8^{+2.9}_{-1.9}$	$0.19^{+0.12}_{-0.11}$
PS1-12bb*	$-17.39^{+0.19}_{-0.16}$	$0.64^{+0.24}_{-0.60}$	$10.02^{+0.85}_{-0.85}$	$-2.71^{+0.23}_{-0.16}$	$1.61^{+0.05}_{-0.04}$	$1.11^{+0.06}_{-0.04}$	$1.61^{+0.28}_{-0.42}$	$0.13^{+0.05}_{-0.05}$	$9.56^{+0.59}_{-0.83}$	$0.35^{+0.11}_{-0.19}$
PS1-12brf	$-19.56^{+0.33}_{-0.38}$	$1.80^{+0.45}_{-0.45}$	$3.16^{+0.60}_{-0.75}$	$-1.27^{+0.26}_{-0.28}$	$1.21^{+0.08}_{-0.10}$	$1.31^{+0.04}_{-0.04}$	$1.11^{+0.62}_{-0.71}$	$0.11^{+0.06}_{-0.04}$	$6.4^{+1.2}_{-0.9}$	$0.11^{+0.11}_{-0.07}$
PS1-12bv	$-20.65^{+0.32}_{-0.39}$	$2.85^{+0.60}_{-0.60}$	$4.8^{+1.2}_{-0.9}$	$-0.76^{+0.20}_{-0.25}$	$0.88^{+0.08}_{-0.08}$	$0.91^{+0.06}_{-0.10}$	$0.3^{+1.2}_{-0.9}$	$0.09^{+0.06}_{-0.03}$	$14.3^{+1.4}_{-1.0}$	$0.18^{+0.10}_{-0.10}$
PS1-13duy	$-20.80^{+0.42}_{-0.36}$	$1.95^{+0.30}_{-0.30}$	$3.31^{+0.90}_{-0.60}$	$-0.81^{+0.31}_{-0.33}$	$0.74^{+0.16}_{-0.18}$	$1.24^{+0.14}_{-0.34}$	$-0.6^{+1.6}_{-0.9}$	$0.13^{+0.05}_{-0.05}$	$6.4^{+2.4}_{-2.3}$	$0.26^{+0.12}_{-0.13}$
PS1-13dwm*	$-18.42^{+0.44}_{-0.56}$	$1.80^{+0.60}_{-0.60}$	$3.2^{+1.1}_{-1.1}$	$-1.17^{+0.32}_{-0.40}$	$1.26^{+0.15}_{-0.19}$	$1.73^{+0.14}_{-0.16}$	$-0.1^{+1.4}_{-1.4}$	$0.11^{+0.06}_{-0.04}$	$6.7^{+2.3}_{-2.5}$	$0.17^{+0.16}_{-0.11}$
PTF10iam	$-20.19^{+0.14}_{-0.13}$	$2.1^{+1.7}_{-0.4}$	$29.5^{+2.6}_{-2.1}$	$-1.54^{+0.15}_{-0.09}$	$0.83^{+0.03}_{-0.03}$	$0.10^{+0.03}_{-0.03}$	$1.83^{+0.13}_{-0.26}$	$0.13^{+0.05}_{-0.05}$	$8.95^{+0.71}_{-0.55}$	$0.40^{+0.07}_{-0.13}$
SNLS04D4ec	$-19.64^{+0.45}_{-0.52}$	$4.0^{+3.4}_{-2.4}$	$6.8^{+4.4}_{-0.8}$	$-1.92^{+0.43}_{-0.33}$	$0.48^{+0.21}_{-0.24}$	$-0.71^{+0.43}_{-0.48}$	$1.40^{+0.37}_{-0.44}$	$0.12^{+0.05}_{-0.05}$	$8.25^{+0.20}_{-0.13}$	$0.05^{+0.08}_{-0.04}$
SNLS05D2bk	$-19.48^{+0.05}_{-0.10}$	$5.02^{+0.25}_{-0.25}$	$12.54^{+0.75}_{-0.50}$	$-0.62^{+0.19}_{-0.21}$	$0.45^{+0.10}_{-0.09}$	$-0.71^{+0.20}_{-0.19}$	$-0.65^{+0.25}_{-0.22}$	$0.11^{+0.06}_{-0.04}$	$7.35^{+0.22}_{-0.19}$	$0.07^{+0.10}_{-0.05}$
SNLS06D1hc	$-19.23^{+0.03}_{-0.07}$	$7.52^{+0.25}_{-0.25}$	$14.54^{+0.50}_{-0.25}$	$-0.02^{+0.12}_{-0.14}$	$0.44^{+0.07}_{-0.07}$	$-0.68^{+0.14}_{-0.13}$	$-1.77^{+0.18}_{-0.15}$	$0.11^{+0.04}_{-0.03}$	$6.48^{+0.11}_{-0.09}$	$0.04^{+0.06}_{-0.03}$
Median	$-19.9^{+1.3}_{-1.0}$	$2.5^{+1.5}_{-1.2}$	$5.0^{+3.6}_{-2.5}$	$-0.95^{+0.48}_{-0.64}$	$0.96^{+0.30}_{-0.28}$	$1.03^{+0.42}_{-0.50}$	$0.6^{+0.7}_{-1.0}$	$0.103^{+0.030}_{-0.033}$	$7.9^{+4.8}_{-2.7}$	$0.15^{+0.18}_{-0.11}$

NOTE—Asterisk (*) marks the FBOT event that lacked the detection epoch before the peak. The values at the last line represent the median with 1σ deviation of each parameter for the collected FBOTs. The columns from left to right are (1) FBOT event; (2) peak absolute magnitude in units of mag; (3) rise time above half-maximum in units of day; (4) decline time above half-maximum in units of day; (5) ejecta mass in units of M_{\odot} ; (6) initial spin period in units of ms; (7) polar magnetic field strength in units of 10^{14} G; (8) opacity to high-energy photons in units of cm^2g^{-1} ; (9) opacity in units of cm^2g^{-1} ; (10) floor temperature in units of 10^3 K; (11) extinction in units of mag.

REFERENCES

- Arcavi, I., Gal-Yam, A., Kasliwal, M. M., et al. 2010, *ApJ*, 721, 777, doi: [10.1088/0004-637X/721/1/777](https://doi.org/10.1088/0004-637X/721/1/777)
- Arcavi, I., Wolf, W. M., Howell, D. A., et al. 2016, *ApJ*, 819, 35, doi: [10.3847/0004-637X/819/1/35](https://doi.org/10.3847/0004-637X/819/1/35)
- Arnett, W. D. 1982, *ApJ*, 253, 785, doi: [10.1086/159681](https://doi.org/10.1086/159681)
- Blanchard, P. K., Berger, E., Nicholl, M., & Villar, V. A. 2020, *ApJ*, 897, 114, doi: [10.3847/1538-4357/ab9638](https://doi.org/10.3847/1538-4357/ab9638)
- Brooks, J., Schwab, J., Bildsten, L., et al. 2017, *ApJ*, 850, 127, doi: [10.3847/1538-4357/aa9568](https://doi.org/10.3847/1538-4357/aa9568)
- Chen, T.-W., Smartt, S. J., Yates, R. M., et al. 2017, *MNRAS*, 470, 3566, doi: [10.1093/mnras/stx1428](https://doi.org/10.1093/mnras/stx1428)
- Chevalier, R. A., & Irwin, C. M. 2011, *ApJL*, 729, L6, doi: [10.1088/2041-8205/729/1/L6](https://doi.org/10.1088/2041-8205/729/1/L6)
- Dai, Z. G., & Lu, T. 1998, *A&A*, 333, L87, <https://arxiv.org/abs/astro-ph/9810402>
- De, K., Kasliwal, M. M., Ofek, E. O., et al. 2018, *Science*, 362, 201, doi: [10.1126/science.aas8693](https://doi.org/10.1126/science.aas8693)
- Drout, M. R., Soderberg, A. M., Mazzali, P. A., et al. 2013, *ApJ*, 774, 58, doi: [10.1088/0004-637X/774/1/58](https://doi.org/10.1088/0004-637X/774/1/58)
- Drout, M. R., Chornock, R., Soderberg, A. M., et al. 2014, *ApJ*, 794, 23, doi: [10.1088/0004-637X/794/1/23](https://doi.org/10.1088/0004-637X/794/1/23)
- Ertl, T., Janka, H. T., Woosley, S. E., Sukhbold, T., & Ugliano, M. 2016, *ApJ*, 818, 124, doi: [10.3847/0004-637X/818/2/124](https://doi.org/10.3847/0004-637X/818/2/124)
- Ertl, T., Woosley, S. E., Sukhbold, T., & Janka, H. T. 2020, *ApJ*, 890, 51, doi: [10.3847/1538-4357/ab6458](https://doi.org/10.3847/1538-4357/ab6458)
- Foreman-Mackey, D., Hogg, D. W., Lang, D., & Goodman, J. 2013, *PASP*, 125, 306, doi: [10.1086/670067](https://doi.org/10.1086/670067)
- Fox, O. D., & Smith, N. 2019, *MNRAS*, 488, 3772, doi: [10.1093/mnras/stz1925](https://doi.org/10.1093/mnras/stz1925)
- Fuller, J., & Lu, W. 2022, *MNRAS*, 511, 3951, doi: [10.1093/mnras/stac317](https://doi.org/10.1093/mnras/stac317)
- Ginzburg, S., & Balberg, S. 2012, *ApJ*, 757, 178, doi: [10.1088/0004-637X/757/2/178](https://doi.org/10.1088/0004-637X/757/2/178)
- Gottlieb, O., Tchekhovskoy, A., & Margutti, R. 2022, *MNRAS*, doi: [10.1093/mnras/stac910](https://doi.org/10.1093/mnras/stac910)
- Ho, A. Y. Q., Phinney, E. S., Ravi, V., et al. 2019, *ApJ*, 871, 73, doi: [10.3847/1538-4357/aaf473](https://doi.org/10.3847/1538-4357/aaf473)
- Ho, A. Y. Q., Perley, D. A., Kulkarni, S. R., et al. 2020, *ApJ*, 895, 49, doi: [10.3847/1538-4357/ab8bcf](https://doi.org/10.3847/1538-4357/ab8bcf)
- Ho, A. Y. Q., Perley, D. A., Gal-Yam, A., et al. 2021, *arXiv e-prints*, arXiv:2105.08811, <https://arxiv.org/abs/2105.08811>
- Hotokezaka, K., Kashiya, K., & Murase, K. 2017, *ApJ*, 850, 18, doi: [10.3847/1538-4357/aa8c7d](https://doi.org/10.3847/1538-4357/aa8c7d)
- Huang, K., Shimoda, J., Urata, Y., et al. 2019, *ApJL*, 878, L25, doi: [10.3847/2041-8213/ab23fd](https://doi.org/10.3847/2041-8213/ab23fd)
- Insera, C. 2019, *Nature Astronomy*, 3, 697, doi: [10.1038/s41550-019-0854-4](https://doi.org/10.1038/s41550-019-0854-4)
- Insera, C., Smartt, S. J., Jerkstrand, A., et al. 2013, *ApJ*, 770, 128, doi: [10.1088/0004-637X/770/2/128](https://doi.org/10.1088/0004-637X/770/2/128)
- Kasen, D., & Bildsten, L. 2010, *ApJ*, 717, 245, doi: [10.1088/0004-637X/717/1/245](https://doi.org/10.1088/0004-637X/717/1/245)
- Kashiya, K., Murase, K., Bartos, I., Kiuchi, K., & Margutti, R. 2016, *ApJ*, 818, 94, doi: [10.3847/0004-637X/818/1/94](https://doi.org/10.3847/0004-637X/818/1/94)
- Kasliwal, M. M., Kulkarni, S. R., Gal-Yam, A., et al. 2010, *ApJL*, 723, L98, doi: [10.1088/2041-8205/723/1/L98](https://doi.org/10.1088/2041-8205/723/1/L98)
- Kremer, K., Lu, W., Piro, A. L., et al. 2021, *ApJ*, 911, 104, doi: [10.3847/1538-4357/abeb14](https://doi.org/10.3847/1538-4357/abeb14)
- Krühler, T., Malesani, D., Fynbo, J. P. U., et al. 2015, *A&A*, 581, A125, doi: [10.1051/0004-6361/201425561](https://doi.org/10.1051/0004-6361/201425561)
- Leung, S.-C., Blinnikov, S., Nomoto, K., et al. 2020, *ApJ*, 903, 66, doi: [10.3847/1538-4357/abba33](https://doi.org/10.3847/1538-4357/abba33)
- Lin, W., Wang, X., Wang, L., & Dai, Z. 2021, *ApJL*, 914, L2, doi: [10.3847/2041-8213/ac004a](https://doi.org/10.3847/2041-8213/ac004a)
- Liu, L.-D., Wang, S.-Q., Wang, L.-J., et al. 2017, *ApJ*, 842, 26, doi: [10.3847/1538-4357/aa73d9](https://doi.org/10.3847/1538-4357/aa73d9)
- Liu, L.-D., Zhang, B., Wang, L.-J., & Dai, Z.-G. 2018, *ApJL*, 868, L24, doi: [10.3847/2041-8213/aaeff6](https://doi.org/10.3847/2041-8213/aaeff6)
- Lü, H.-J., Lan, L., Zhang, B., et al. 2018, *ApJ*, 862, 130, doi: [10.3847/1538-4357/aacd03](https://doi.org/10.3847/1538-4357/aacd03)
- Lü, H.-J., & Zhang, B. 2014, *ApJ*, 785, 74, doi: [10.1088/0004-637X/785/1/74](https://doi.org/10.1088/0004-637X/785/1/74)
- Lunnan, R., Chornock, R., Berger, E., et al. 2014, *ApJ*, 787, 138, doi: [10.1088/0004-637X/787/2/138](https://doi.org/10.1088/0004-637X/787/2/138)
- Lyman, J. D., Bersier, D., James, P. A., et al. 2016, *MNRAS*, 457, 328, doi: [10.1093/mnras/stv2983](https://doi.org/10.1093/mnras/stv2983)
- Margutti, R., Metzger, B. D., Chornock, R., et al. 2019, *ApJ*, 872, 18, doi: [10.3847/1538-4357/aafa01](https://doi.org/10.3847/1538-4357/aafa01)
- Mazzali, P. A., McFadyen, A. I., Woosley, S. E., Pian, E., & Tanaka, M. 2014, *MNRAS*, 443, 67, doi: [10.1093/mnras/stu1124](https://doi.org/10.1093/mnras/stu1124)
- Metzger, B. D. 2022, *arXiv e-prints*, arXiv:2203.04331, <https://arxiv.org/abs/2203.04331>
- Metzger, B. D., Margalit, B., Kasen, D., & Quataert, E. 2015, *MNRAS*, 454, 3311, doi: [10.1093/mnras/stv2224](https://doi.org/10.1093/mnras/stv2224)
- Milisavljevic, D., Soderberg, A. M., Margutti, R., et al. 2013, *ApJL*, 770, L38, doi: [10.1088/2041-8205/770/2/L38](https://doi.org/10.1088/2041-8205/770/2/L38)
- Mohan, P., An, T., & Yang, J. 2020, *ApJL*, 888, L24, doi: [10.3847/2041-8213/ab64d1](https://doi.org/10.3847/2041-8213/ab64d1)
- Mor, R., Livne, E., & Piran, T. 2022, *arXiv e-prints*, arXiv:2203.08292, <https://arxiv.org/abs/2203.08292>
- Moriya, T. J., & Eldridge, J. J. 2016, *MNRAS*, 461, 2155, doi: [10.1093/mnras/stw1471](https://doi.org/10.1093/mnras/stw1471)
- Nicholl, M., Guillochon, J., & Berger, E. 2017, *ApJ*, 850, 55, doi: [10.3847/1538-4357/aa9334](https://doi.org/10.3847/1538-4357/aa9334)

- Pellegrino, C., Howell, D. A., Vinkó, J., et al. 2022, ApJ, 926, 125, doi: [10.3847/1538-4357/ac3e63](https://doi.org/10.3847/1538-4357/ac3e63)
- Perley, D. A., Tanvir, N. R., Hjorth, J., et al. 2016, ApJ, 817, 8, doi: [10.3847/0004-637X/817/1/8](https://doi.org/10.3847/0004-637X/817/1/8)
- Perley, D. A., Mazzali, P. A., Yan, L., et al. 2019, MNRAS, 484, 1031, doi: [10.1093/mnras/sty3420](https://doi.org/10.1093/mnras/sty3420)
- Pian, E., Mazzali, P. A., Moriya, T. J., et al. 2020, MNRAS, 497, 3542, doi: [10.1093/mnras/staa2191](https://doi.org/10.1093/mnras/staa2191)
- Piro, A. L., & Ott, C. D. 2011, ApJ, 736, 108, doi: [10.1088/0004-637X/736/2/108](https://doi.org/10.1088/0004-637X/736/2/108)
- Prentice, S. J., Maguire, K., Smartt, S. J., et al. 2018, ApJL, 865, L3, doi: [10.3847/2041-8213/aadd90](https://doi.org/10.3847/2041-8213/aadd90)
- Pursiainen, M., Childress, M., Smith, M., et al. 2018, MNRAS, 481, 894, doi: [10.1093/mnras/sty2309](https://doi.org/10.1093/mnras/sty2309)
- Radice, D., Perego, A., Hotokezaka, K., et al. 2018, ApJ, 869, 130, doi: [10.3847/1538-4357/aaf054](https://doi.org/10.3847/1538-4357/aaf054)
- Rest, A., Garnavich, P. M., Khatami, D., et al. 2018, Nature Astronomy, 2, 307, doi: [10.1038/s41550-018-0423-2](https://doi.org/10.1038/s41550-018-0423-2)
- Rivera Sandoval, L. E., Maccarone, T. J., Corsi, A., et al. 2018, MNRAS, 480, L146, doi: [10.1093/mnrasl/sly145](https://doi.org/10.1093/mnrasl/sly145)
- Saito, S., Tanaka, M., Sawada, R., & Moriya, T. J. 2022, arXiv e-prints, arXiv:2205.00624. <https://arxiv.org/abs/2205.00624>
- Sawada, R., Kashiyama, K., & Suwa, Y. 2022, ApJ, 927, 223, doi: [10.3847/1538-4357/ac53ae](https://doi.org/10.3847/1538-4357/ac53ae)
- Schlafly, E. F., & Finkbeiner, D. P. 2011, ApJ, 737, 103, doi: [10.1088/0004-637X/737/2/103](https://doi.org/10.1088/0004-637X/737/2/103)
- Soker, N. 2022, Research in Astronomy and Astrophysics, 22, 055010, doi: [10.1088/1674-4527/ac5b40](https://doi.org/10.1088/1674-4527/ac5b40)
- Soker, N., Grichener, A., & Gilkis, A. 2019, MNRAS, 484, 4972, doi: [10.1093/mnras/stz364](https://doi.org/10.1093/mnras/stz364)
- Suwa, Y., Yoshida, T., Shibata, M., Umeda, H., & Takahashi, K. 2015, MNRAS, 454, 3073, doi: [10.1093/mnras/stv2195](https://doi.org/10.1093/mnras/stv2195)
- Taddia, F., Sollerman, J., Fremling, C., et al. 2019, A&A, 621, A71, doi: [10.1051/0004-6361/201834429](https://doi.org/10.1051/0004-6361/201834429)
- Tampo, Y., Tanaka, M., Maeda, K., et al. 2020, ApJ, 894, 27, doi: [10.3847/1538-4357/ab7ccc](https://doi.org/10.3847/1538-4357/ab7ccc)
- Tauris, T. M., Langer, N., Moriya, T. J., et al. 2013, ApJL, 778, L23, doi: [10.1088/2041-8205/778/2/L23](https://doi.org/10.1088/2041-8205/778/2/L23)
- Tauris, T. M., Langer, N., & Podsiadlowski, P. 2015, MNRAS, 451, 2123, doi: [10.1093/mnras/stv990](https://doi.org/10.1093/mnras/stv990)
- Tauris, T. M., Kramer, M., Freire, P. C. C., et al. 2017, ApJ, 846, 170, doi: [10.3847/1538-4357/aa7e89](https://doi.org/10.3847/1538-4357/aa7e89)
- Ugliano, M., Janka, H.-T., Marek, A., & Arcones, A. 2012, ApJ, 757, 69, doi: [10.1088/0004-637X/757/1/69](https://doi.org/10.1088/0004-637X/757/1/69)
- Wang, S.-Q., Gan, W.-P., Li, L., et al. 2019, arXiv e-prints, arXiv:1904.09604. <https://arxiv.org/abs/1904.09604>
- Wheeler, J. C., Yi, I., Höflich, P., & Wang, L. 2000, ApJ, 537, 810, doi: [10.1086/309055](https://doi.org/10.1086/309055)
- Whitesides, L., Lunnan, R., Kasliwal, M. M., et al. 2017, ApJ, 851, 107, doi: [10.3847/1538-4357/aa99de](https://doi.org/10.3847/1538-4357/aa99de)
- Wiseman, P., Pursiainen, M., Childress, M., et al. 2020, MNRAS, 498, 2575, doi: [10.1093/mnras/staa2474](https://doi.org/10.1093/mnras/staa2474)
- Woosley, S. E. 2010, ApJL, 719, L204, doi: [10.1088/2041-8205/719/2/L204](https://doi.org/10.1088/2041-8205/719/2/L204)
- Xiang, D., Wang, X., Lin, W., et al. 2021, ApJ, 910, 42, doi: [10.3847/1538-4357/abdeba](https://doi.org/10.3847/1538-4357/abdeba)
- Yu, Y.-W., Chen, A., & Li, X.-D. 2019a, ApJL, 877, L21, doi: [10.3847/2041-8213/ab1f85](https://doi.org/10.3847/2041-8213/ab1f85)
- Yu, Y.-W., Chen, A., & Wang, B. 2019b, ApJL, 870, L23, doi: [10.3847/2041-8213/aaf960](https://doi.org/10.3847/2041-8213/aaf960)
- Yu, Y.-W., Cheng, K. S., & Cao, X.-F. 2010, ApJ, 715, 477, doi: [10.1088/0004-637X/715/1/477](https://doi.org/10.1088/0004-637X/715/1/477)
- Yu, Y.-W., Li, S.-Z., & Dai, Z.-G. 2015, ApJL, 806, L6, doi: [10.1088/2041-8205/806/1/L6](https://doi.org/10.1088/2041-8205/806/1/L6)
- Yu, Y.-W., Zhang, B., & Gao, H. 2013, ApJL, 776, L40, doi: [10.1088/2041-8205/776/2/L40](https://doi.org/10.1088/2041-8205/776/2/L40)
- Yu, Y.-W., Zhu, J.-P., Li, S.-Z., Lü, H.-J., & Zou, Y.-C. 2017, ApJ, 840, 12, doi: [10.3847/1538-4357/aa6c27](https://doi.org/10.3847/1538-4357/aa6c27)
- Zenati, Y., Perets, H. B., & Toonen, S. 2019, MNRAS, 486, 1805, doi: [10.1093/mnras/stz316](https://doi.org/10.1093/mnras/stz316)
- Zhang, B. 2018, The Physics of Gamma-Ray Bursts, doi: [10.1017/9781139226530](https://doi.org/10.1017/9781139226530)
- Zhang, B., & Mészáros, P. 2001, ApJL, 552, L35, doi: [10.1086/320255](https://doi.org/10.1086/320255)
- Zhang, Z.-D., Yu, Y.-W., & Liu, L.-D. 2022, arXiv e-prints, arXiv:2204.11092. <https://arxiv.org/abs/2204.11092>
- Zhu, J.-P., Yang, Y.-P., Zhang, B., et al. 2021a, ApJL, 914, L19, doi: [10.3847/2041-8213/abff5a](https://doi.org/10.3847/2041-8213/abff5a)
- Zhu, J.-P., Zhang, B., Yu, Y.-W., & Gao, H. 2021b, ApJL, 906, L11, doi: [10.3847/2041-8213/abd412](https://doi.org/10.3847/2041-8213/abd412)